FULL PAPER

Dalton
www.rsc.org/dalton

Metal complexes of a dipyridine octaazamacrocycle: stability constants, structural and modelling studies

Carla Cruz,[a] Sílvia Carvalho,[b] Rita Delgado,[b,c] Michael G. B. Drew,[d] Vítor Félix[a] and Brian J. Goodfellow[a]

[a] *Departamento Química, CICECO, Universidade de Aveiro, 3810-193 Aveiro, Portugal*
[b] *Instituto de Tecnologia Química e Biológica, UNL, Apartado 127, 2781-901 Oeiras, Portugal*
[c] *Instituto Superior Técnico, Av. Rovisco Pais, 1049-001 Lisboa, Portugal*
[d] *Department of Chemistry, University of Reading, Whiteknights, Reading, UK RG6 6AD*

Received 22nd April 2003, Accepted 26th June 2003
First published as an Advance Article on the web 17th July 2003

Two 28-membered octaazamacrocycles, [28]py_2N_6 and Me_2[28]py_2N_6, have been synthesized. The protonation constants of the *N*-methyl derivative and the stability constants of its complexes with Ni^{2+}, Cu^{2+}, Zn^{2+}, Cd^{2+}, and Pb^{2+} were determined at 25 °C in 0.10 mol dm^{-3} KNO_3. The high overall basicity of Me_2[28]py_2N_6 is ascribed to the weaker repulsion between protonated contiguous charged ammonium sites separated by propyl chains. These studies together with NMR, UV-vis and EPR spectroscopies indicated the presence of mono- and di-nuclear species. The single crystal structure of the complex $[Ni_2([28]py_2N_6)(H_2O)_4]Cl_4 \cdot 3H_2O$ was determined, and showed each nickel centre in a distorted octahedral co-ordination environment. The nickel centres are held within the macrocycle at a large distance of 6.991(8) Å from each other. The formation of mononuclear complexes was evaluated theoretically *via* molecular mechanics (MM) and molecular dynamics (MD) calculations and showed that these large macrocycles have sufficient flexibility to encapsulate metal ions with different stereo-electronic sizes. Structures for small and large metal ions are proposed.

Introduction

Octaazamacrocycles exhibit interesting co-ordination properties because in spite of the large cavity size formed by the macrocyclic backbone, they are capable of forming stable mono- and di-nuclear metal complexes, as well as stabilizing various anions in their hexaprotonated form.[1,2]

Recently we have studied the 18- and 20-membered hexaazamacrocycles, [18]py_2N_4 and [20]py_2N_4 (see Scheme 1), which form very stable mononuclear complexes. The metals are encapsulated in hexa-co-ordinate environments, the macrocycles adopting a twisted helical topology.[3] In spite of the dimensions of both macrocycles their cavities are too small to incorporate two metal centres without the folding of the macrocycle. In fact, to the best of our knowledge, dinuclear complexes with [18]py_2N_4 and [20]py_2N_4 are not to be found in the Cambridge Structural Data Base (CSD).[4] One X-ray structure of a homodinuclear copper(II) complex was determined, $[Cu_2([20]py_2N_4])(H_2O)_4]^{4+}$, but has not yet been published,[5] and as expected the macrocycle exhibits a cleft conformation with each metal bonded in an exocyclic manner (outside the macrocyclic cavity) to the three nitrogen atoms of the head of the macrocycle in a distorted square pyramidal environment.

Searching for macrocycles able to accommodate two metal centres we have synthesized two 28-membered octaazamacrocycles, 3,7,11,19,23,27,33,34-octaazatricyclo[27.3.1.1^{13,17}]tetratriacontane-1(32),13(14),15,17,29,31-hexaene ([28]py_2N_6) and its 7,23-dimethyl-derivative, Me_2[28]py_2N_6, see Scheme 1. In this context, we are also interested in determining the critical size of the spacer between the two –$HNCH_2$(py)CH_2NH– moieties which will allow two metal centres to be encapsulated within the macrocycle.

In the present work the co-ordination behaviour of [28]py_2N_6 and Me_2[28]py_2N_6 was studied and the formation of mono- and di-nuclear complexes was investigated, using a plethora of methods, including potentiometric measurements, such as NMR, UV-vis, EPR spectroscopies and X-ray single crystal diffraction. The mononuclear species were also investigated by molecular mechanics (MM) and molecular dynamics (MD) calculations.

Results and discussion

Synthesis of macrocycles

The compounds Me_2[28]py_2N_6 and [28]py_2N_6 were prepared in good yield by a [2 + 2] condensation of 2,6-pyridinedicarbaldehyde and the appropriate triamine [3,3-diamine-*N*-methyldipropylamine or bis(3-aminopropyl)amine], followed by the reduction of the Schiff base. This procedure has been used before to prepare [28]py_2N_6[6] and the related tetraimine compound.[7] A 20-membered tetraimine macrocycle (Schiff base) in the contracted form was obtained when bis(3-aminopropyl)-amine was used, as confirmed by an X-ray crystal structure determination. However, this structure had already been determined.[7] The contracted form is obtained when the imine group of the extended Shiff-base macrocycle is attacked by the adjacent amine. The oxidation of the dinuclear Cu(I) complex of the contracted ring macrocycle results in the expanded Cu(II) dinuclear complex.[7] Compounds [28]py_2N_6 and Me_2[28]py_2N_6 were also synthesized using Pb^{2+} as the template ion,[8] although at much lower yield in our hands, because Pb^{2+} was hard to remove from the complex. The pure compounds were obtained as salts by precipitation of the hexaprotonated hydrochloride.

Nelson *et al.* found that the condensation of 2,6-pyridinedicarbaldehyde and $H_2N(CH_2)_3N(R)(CH_2)_3NH_2$ in the presence of Mn^{2+}, Co^{2+}, Ni^{2+}, Cu^{2+} or Zn^{2+} (R = Me) or Ca^{2+} and Sr^{2+} (R = H) led to mononuclear metal complexes,[9,10] while dinuclear complexes of the tetraimine Shiff-base were formed in the presence of Ag^+ and Pb^{2+} (R = Me).[10] It was also shown that the fully expanded form was obtained when Ag^+ was used as the template metal, whereas the use of smaller ions such as Ca^{2+} and Sr^{2+} produced the ring contracted form.[11] This ring-contraction has also been observed in the synthesis of Me_4[22]py_2N_6, for which the X-ray crystal structure of its Ba^{2+} complex was determined.[12]

Acid–base behaviour

The acid–base reactions of Me_2[28]py_2N_6 were studied by potentiometric methods. The protonation constants deter-

DOI: 10.1039/b304381a

Table 1 Protonation (log K_i^H) constants of $Me_2[28]py_2N_6$, $[24]py_2N_6$ and $[24]N_8$ (T = 25.0 °C; I = 0.10 mol dm^{-3} in KNO_3)

Ion	Equilibrium quotient	$Me_2[28]py_2N_6$ [a]	$[24]py_2N_6$ [b]	$[24]N_8$ [c]	$[24]N_8$ [d]
H^+	[HL]/[L]×[H]	9.87(1)	9.25	10.01	9.65
	$[H_2L]/[HL]\times[H]$	9.18(1)	8.49	9.50	9.33
	$[H_3L]/[H_2L]\times[H]$	8.30(1)	7.55	9.10	8.76
	$[H_4L]/[H_3L]\times[H]$	7.63(2)	6.98	8.29	7.87
	$[H_5L]/[H_4L]\times[H]$	6.83(2)	4.11	5.01	4.55
	$[H_6L]/[H_5L]\times[H]$	6.32(2)	3.26	3.71	3.42
	$[H_7L]/[H_6L]\times[H]$	3.21(3)	–	2.98	2.71
	$[H_8L]/[H_7L]\times[H]$	2.81(3)	–	1.97	1.95
	$[H_6L]/[L]\times[H]$ [6]	48.13(1)	39.64	45.62	43.58

[a] Values in parentheses are standard deviations in the last significant figures. [b] I = 0.100 mol dm^{-3} in KCl, ref. 13. [c] I = 0.5 mol dm^{-3} in $NaClO_4$, ref. 14. [d] I = 0.15 mol dm^{-3} in $NaClO_4$, ref. 15.

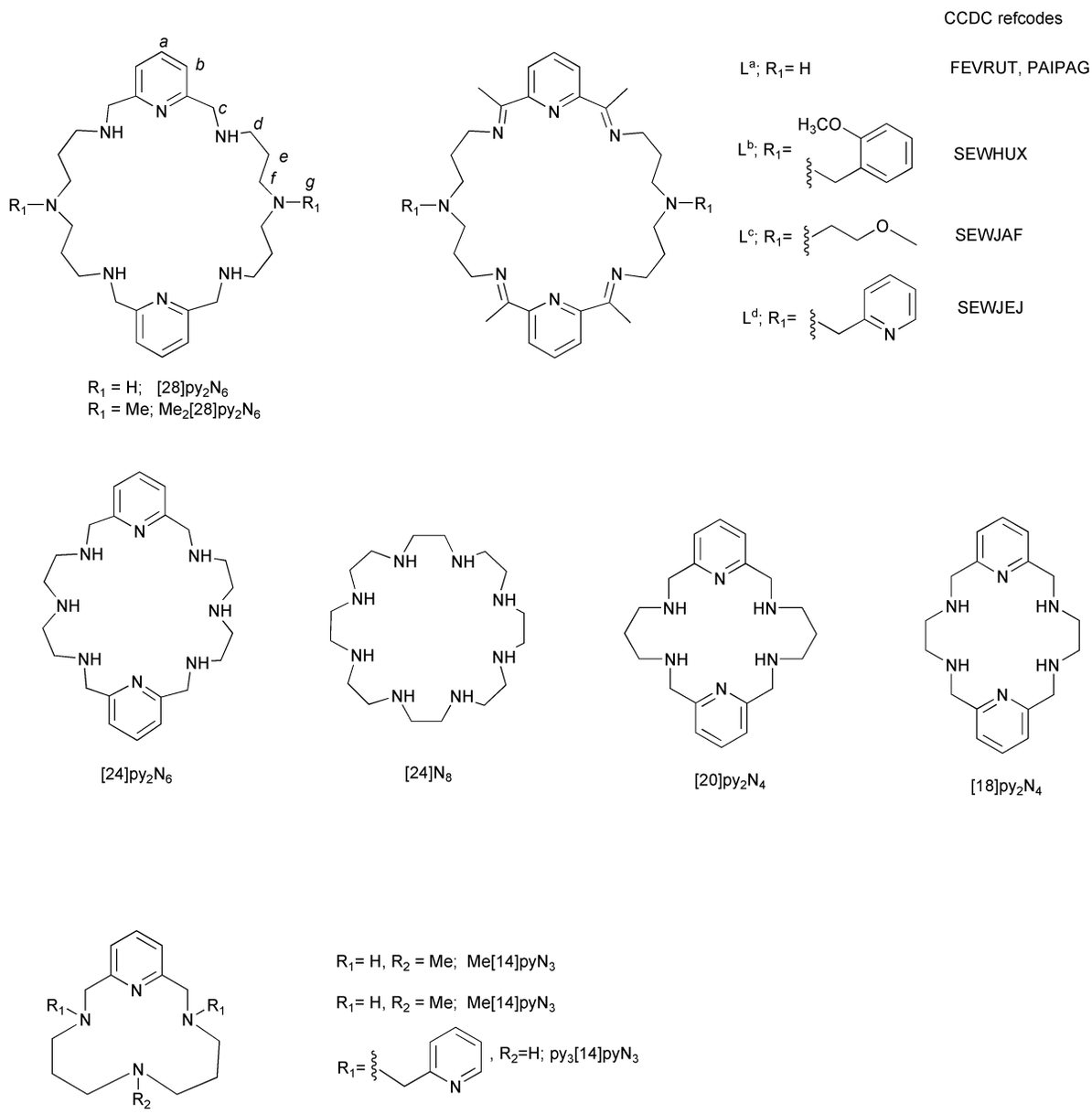

Scheme 1

mined are collected in Table 1 together with the constants for $[24]py_2N_6$ [13] and $[24]N_8$ [14] for comparison.

It was possible to determine all the protonation constants, corresponding to the eight basic centres of $Me_2[28]py_2N_6$ using potentiometry. This compound has the highest overall basicity among those listed in Table 1 due to the moderate repulsion of consecutive protonated amine centres, separated by propyl chains, rather than ethyl chains in $[24]py_2N_6$ and $[24]N_8$. The first four protonation constants of these three compounds are less sensitive to the distance between nitrogen donors, because they correspond to the protonation of amine centres far from each other, and as such they are of the order of those for linear amines.[15] However, the fifth and subsequent constants correspond to protonations of consecutive amine centres, and the basicity of these centres is correlated with the length of the hydrocarbon chain between amines. Therefore $Me_2[28]py_2N_6$ provides the highest values for constants K_5 to K_8. The first four protonation constants of $Me_2[28]py_2N_6$ are slightly higher than

Table 2 Stability constants (log $\beta_{M_mH_hL_l}$ or log $K_{M_mH_hL_l}$)[a] of the complexes of $Me_2[28]py_2N_6$, $[24]py_2N_6$ and $[24]N_8$ with several divalent metal ions. T = 25.0 °C; I = 0.10 mol dm^{-3} in KNO_3

Ion	Species *mhl*	$Me_2[28]py_2N_6$[b] log $\beta_{M_mH_hL_l}$	log $K_{M_mH_hL_l}$	$[24]py_2N_6$[c] log $K_{M_mH_hL_l}$	$[24]N_8$[d] log $K_{M_mH_hL_l}$
Ni^{2+}	101	10.58(2)	10.58	–	13.94
	111	19.36(2)	8.78		9.09
	121	26.51(3)	7.15		7.23
	131	33.57(3)	7.06		–
	141	40.17(1)	6.60		–
	201	15.09(3)	4.52		9.36
	211	23.05(3)	7.96		–
	221	30.48(2)	7.43		–
	2−11	[6.4(1)][e]	[−9.0][e]		−10.11
	2−21	[−2.6(1)][e]	[−9.5][e]		
Cu^{2+}	101	16.30(6)	16.30	20.90	–
	111	25.42(5)	9.12	7.14	–
	121	32.83(5)	7.41	–	–
	131	39.32(5)	6.49	–	–
	141	44.78(1)	5.46	–	–
	1−11	5.57(8)	−10.73	–	–
	201	28.48(2)	12.18	12.58	35.25[f]
	211	34.75(3)	6.27	–	2.90
	221	40.70(1)	5.95	–	–
	2−11	20.16(3)	–8.32	−9.28	−9.00
	2−21	9.82(4)	−10.34	−10.59	–
Zn^{2+}	101	10.36(2)	10.35	–	13.49
	111	18.75(1)	8.52		8.58
	121	25.60(1)	6.64		5.53
	141	38.55(1)	–		–
	1−11	–	–		−10.69
	2−11	6.16(2)	–		12.60[f]
	2−21	−1.93(2)	–		3.0[f]
Cd^{2+}	101	8.22(2)	8.22		14.52
	111	17.50(1)	9.28		7.15
	121	25.03(2)	7.54		5.86
	131	32.07(2)	7.03		–
	141	38.82(1)	6.76		–
	201	12.10(4)	3.88		3.69
	211	20.58(4)	8.48		–
	221	28.51(2)	7.93		–
	2−11	3.37(2)	−8.73		–
Pb^{2+}	101	–		–	10.83
	111	16.04(7)			8.65
	121	24.50(4)	8.46		7.44
	131	32.12(3)	7.62		4.76
	141	38.85(1)	6.74		–
	201	13.49(2)	–		6.74
	211	21.32(2)	7.83		6.16
	2−11	5.04(2)	−8.45		−9.8
	2−21	−3.98(1)	−9.02		–

[a] See Experimental section, Calculation of stability constants, for definitions. [b] Values in parenthesis are standard deviations in the last significant figures. [c] I = 0.100 mol dm^{-3} KCl, ref. 13. [d] I = 0.15 mol dm^{-3} $NaClO_4$, ref. 15. [e] Values with less accuaracy, determined with few points, due to precipitation. [f] log $\beta_{M_mH_hL_l}$.

those of $[24]py_2N_6$ for the same reasons, but lower than those of $[24]N_8$ taking into account the electron withdrawing effect of the pyridine rings of the first two compounds.

Metal complex studies

The stability constants of $Me_2[28]py_2N_6$ with Ni^{2+}, Cu^{2+}, Zn^{2+}, Cd^{2+} and Pb^{2+} metal ions were also determined and the results are collected in Table 2, together with those for $[24]py_2N_6$ (only values for the Cu^{2+} complexes are available)[13] and $[24]N_8$[2,14,15] for comparison. The titration curves for 1 : 1 (metal : ligand) ratios are reproduced in Fig. 1. As expected of a ligand with eight donor atoms, several complexes were found in solution with the divalent metal ions studied: mononuclear [ML^{2+}, MH_iL^{i+2} (i = 1–4), $ML(OH)^+$] and dinuclear [M_2L^{4+}, $M_2H_jL^{4+j}$ (j = 1, 2), $M_2L(OH)_k^{4-k}$, k = 1, 2], where L = $Me_2[28]py_2N_6$. This is illustrated in the speciation diagram[16] shown in Fig. 2 for the Ni^{2+} complexes. It was impossible to determine the constant corresponding to the formation of Zn_2L^{4+} (or other dinuclear protonated complexes) due to the immediate hydrolysis of water molecules giving $Zn_2L(OH)^{3+}$ and $Zn_2L(OH)_2^{2+}$ which start to form at pH values *ca.* 7. The stability constant corresponding to PbL^{2+} was also not available, due to the much more stable Pb_2L^{4+} and the two hydrolysed species, $Pb_2L(OH)^{3+}$ and $Pb_2L(OH)_2^{2+}$ being formed even at a 1 : 1 ratio. Accurate values for the constants of the two hydrolysed species, $Ni_2L(OH)^{3+}$ and $Ni_2L(OH)_2^{2+}$ could not be determined due to precipitation.

Four MH_iL species were found, with partial stability constants between 5.5 and 9.3 (log units). The consecutive deprotonations of MH_4L^{6+} are quite insensitive to the type of metal, but the sequence of deprotonation is difficult to predict even on the basis of an acid–base titration followed by NMR spectroscopy (see below), because all the protonation constants are close to each other and consequently two or three deprotonations occur simultaneously depending on the pH (see Fig. 2). Whatever the identity of the protonation sites the formation of mononuclear complexes requires the folding of the

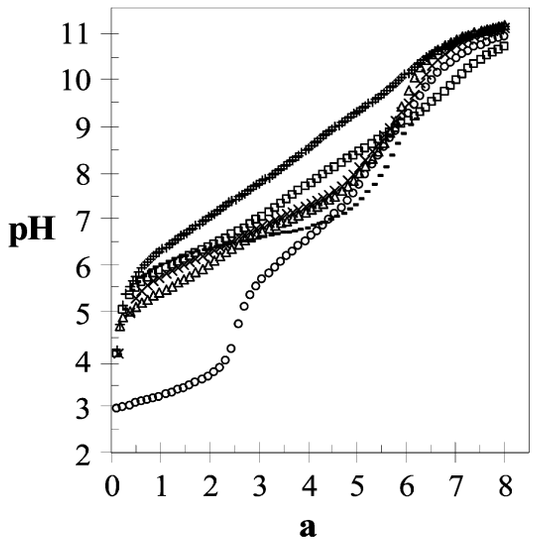

Fig. 1 Titration curves, of *a versus* pH, for the ligand $Me_2[28]py_2N_6$ (+) and the ligand with Cu^{2+} (○), Zn^{2+} (–), Ni^{2+} (△), Pb^{2+} (□) and Cd^{2+} (×) in a 1 : 1 ratio (*a* being the number of moles of base per mole of ligand).

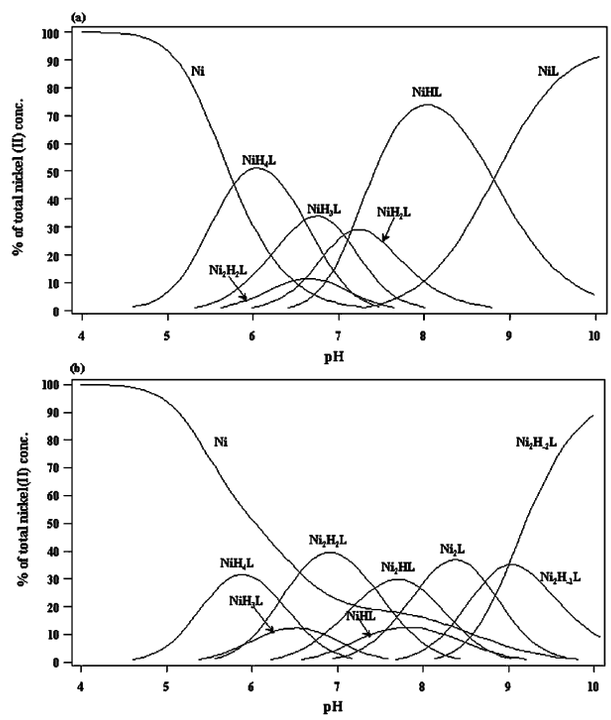

Fig. 2 Species distribution curves calculated for the Ni(II) : $Me_2[28]py_2N_6$ complexes: (a) 1 : 1 ratio, $c_L = c_M = 1.40 \times 10^{-3}$ mol dm^{-3} and (b) 2 : 1 ratio (M : L), $c_L = 1.40 \times 10^{-3}$ mol dm^{-3} and $c_M = 2.80 \times 10^{-3}$ mol dm^{-3}.

macrocycle. The conformational energy required for this folding seems not to be compensated for by the formation of the ML^{2+} complex when M = Pb which prefers to form dinuclear species.

The comparison with the other octaazamacrocycles (Table 2) shows that the complexes formed by $Me_2[28]py_2N_6$ are thermodynamically less stable in spite of its higher basicity. This observation is expected because several six-membered chelate rings are formed on complexation to the metal compared to the five-membered chelate rings formed by the other ligands. However these differences are attenuated when the dinuclear complexes are compared and even inverted for the Pb^{2+} complexes in the case of $[24]N_8$, which is the only ligand for which stability constants are well established.

Table 3 Selected bond distances (Å) and angles (°) in the metal co-ordination sphere of $[Ni_2([28]py_2N_6)(H_2O)_4]^{4+}$, **1**

Ni–N(3)	2.057(10)	Ni–N(7)	2.087(11)
Ni–N(10)	1.990(11)	Ni–N(16)	2.227(11)
Ni–O(100)	2.100(11)	Ni–O(200)	2.188(13)
O(100)–Ni–O(200)	178.7(4)		
N(10)–Ni–N(3)	174.8(5)	N(7)–Ni–N(16)	157.3(5)
N(10)–Ni–N(7)	79.3(4)	N(10)–Ni–N(16)	78.0(4)
N(3)–Ni–N(16)	106.2(4)	N(3)–Ni–N(7)	96.5(4)
N(10)–Ni–O(100)	93.3(5)	N(3)–Ni–O(100)	89.5(5)
N(7)–Ni–O(100)	86.5(5)	N(10)–Ni–O(200)	87.9(5)
N(3)–Ni–O(200)	89.2(5)	N(7)–Ni–O(200)	93.3(5)
O(100)–Ni–N(16)	94.1(5)	O(200)–Ni–N(16)	86.6(5)

Structural studies

Crystallographic studies. The overall geometry of the $[Ni_2([28]py_2N_6)(H_2O)_4]^{4+}$ cation, **1**, is shown in Fig. 3 together with the atom notation scheme adopted. The selected distances and angles are given in Table 3. The cation has a crystallographic inversion centre. In the asymmetric unit there are also two water molecules of solvation and two chlorides as counter-ions. The two anions and one water are located in independent crystallographic positions while the remaining water is located on a 2 fold axis leading to the molecular formula $[Ni_2([28]py_2N_6)(H_2O)_4]Cl_4 \cdot 3H_2O$. Each nickel centre displays a distorted octahedral co-ordination environment with the equatorial plane defined by four sequential nitrogen atoms of the macrocycle, as shown in Fig. 3. The axial positions are occupied by two oxygen atoms from water molecules with Ni–O distances of 2.100(11) and 2.188(13) Å. The Ni–N distance to the pyridine ring is shorter [1.990(11) Å] than those to the secondary amino nitrogens [2.057(10), 2.087(11) and 2.227(11) Å], as would be expected for complexes containing the pyridyl structural moieties.[3,17] The longest Ni–N distance found involves one of the two nitrogen atoms contiguous to the pyridine ring. The macrocycle adopts a ladder type conformation (see Fig. 3) with each pyridyl ring slightly tilted by 13.3(4)° relatively to the N_4 equatorial co-ordination plane. The two pyridine rings are perforce parallel as a consequence of the C_i crystallographic symmetry. The distance of the nickel from the N_4 co-ordination plane is only 0.027(8) Å, indicating that the metal is barely out of the macrocyclic cavity. The Ni ··· Ni distance within the macrocycle is 6.991(8) Å.

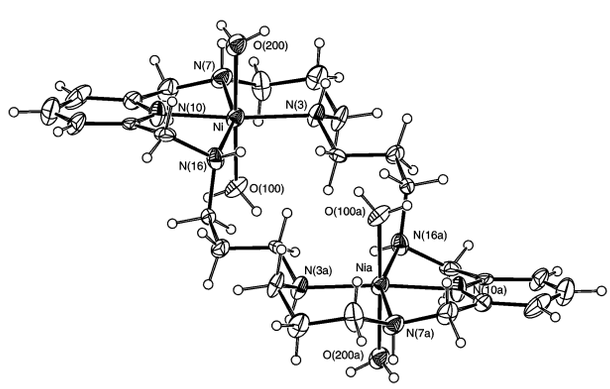

Fig. 3 ORTEP diagram showing the overall structure of the $[Ni_2([28]py_2N_6)(H_2O)_4]^{4+}$ cation (ellipsoids drawn at 30% level). The labelling scheme adopted for the carbon atoms is omitted for clarity. The symmetry operation to generate the equivalent atoms: a $1/2 - x$, $1/2 - y$, $-z$.

To the best of our knowledge, **1** is the first X-ray determination of a complex of $[28]py_2N_6$. Indeed, no structures with this ligand were found in a search for similar structures in the CSD.[4] However, five X-ray structures of 28-membered related macrocyclic complexes containing diimine pyridyl heads connected by two *N*,*N*-propylamine spacers were found: $[Cu_2L^a(HNCS)_2]^{4+}$

Table 4 Dimensions of hydrogen bonds in complex **1**

	H ··· A /Å	D ··· A /Å	D–H ··· A /°[a]
N(3)–H(3) ··· Cl(2) [x, y, $1+z$]	2.42	3.33(2)	176
N(7)–H(7) ··· Cl(1)	2.57	3.40(2)	153
N(16) –H(16) ··· Cl(2) [$1/2 - x$, $1/2 - y$, $-z$]	2.72	3.62(2)	170
O(100)–H(101) ··· Cl(1) [x, y, $-1 + z$]	2.30	3.11(1)	168
O(100)–H(102) ··· Cl(2)	2.50	3.23(1)	149
O(200)–H(202) ··· Cl(2) [x, y, $1 + z$]	2.41	3.21(1)	167
O(200)–H(201) ··· Cl(1)	2.35	3.16(1)	172
O(300)–H(301) ··· Cl(1)	2.54	3.22(1)	140
O(400)–H(401) ··· O(300) [$-x$, $1 - y$, $1 - z$]	2.03	2.80(2)	156

[a] A and D denote the acceptor and the donor, respectively.

(**2**, refcode FEVRUT), $[Ag_2L^a]^{2+}$ (**3**, refcode PAIPAG), $[Ag_2L^b]^{2+}$ (**4**, refcode SEWHUX), $[Ag_2L^c]^{2+}$ (**5**, refcode SEWJAF) and $[Ag_2L^d]^{2+}$ (**6**, refcode SEWJEJ). Molecular diagrams of these complexes showing their overall geometries are presented in Fig. 4 and the structure of ligands in Scheme 1. The copper complex **2** and silver complexes **3** and **4** display symmetric co-ordination modes, with each metal centre located at the end of the macrocycle and surrounded by four nitrogen atoms leading to M ··· M distances of 7.250 Å in **2**, 6.004 Å in **3** and 5.828 Å in **4**. In complex **6** the two silver centres are also located at the extremes of the macrocycle but with the nitrogen atom of one imine group replaced by the nitrogen atom of the *N*-pyridyl arm in the metal co-ordination sphere, and a long distance between the two Ag^+ centres was also found (6.824 Å). By contrast the dinuclear complex **5** exhibits an asymmetric co-ordination mode with the two silver centers having three- and five-co-ordination, respectively. A pair of imino groups co-ordinate asymmetrically the two metal centers and a remarkably short Ag ··· Ag distance of 2.908 Å is observed.

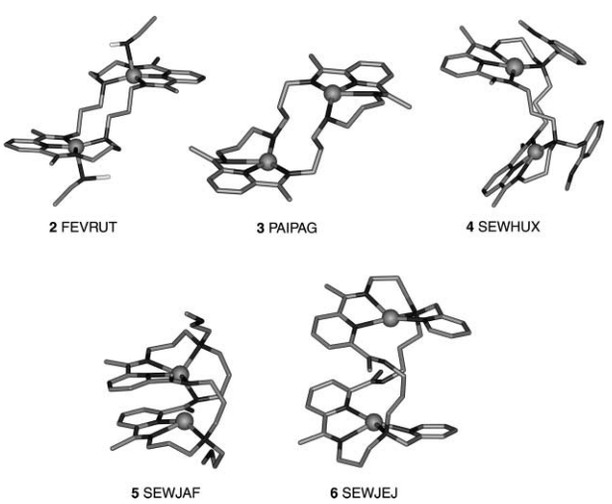

Fig. 4 Molecular diagrams showing the co-ordination modes and the conformations of 28-membered octaazamacrocycles in related dinuclear complexes. Hydrogen atoms bonded to carbon atoms are omitted for clarity.

Furthermore, the macrocyle in **4**–**6** adopts a concertina conformation while **2** and **3** show ladder type conformations, such as is found for **1**, with the pyridyl rings in anti-periplanar arrangements making a dihedral angle of 0°. This comparison suggests, therefore, that the distance between the two metal centers is basically governed by the co-ordination mode. In other words the electronic communication between the two metal centers requires an asymmetric co-ordination mode or alternatively a bridging ligand, which forces the approach of the two metal centers. The theoretical study of the co-ordination of $[28]py_2N_6$ and related macrocycles with larger dimensions in dinuclear complexes is in progress.

The view of the crystal-packing diagram along the *b* crystallographic axis, presented in Fig. 5, shows that the two chloride counter-ions are involved in hydrogen bonding interactions with co-ordinated water molecules from neighbouring complexes forming a four-membered ring. Concomitantly the chloride anions interact with the N–H groups of macrocycles of adjacent complexes, leading to the formation of a 2-D hydrogen bonding network. Furthermore the two crystallization water molecules form water bridges, which also interact with the chloride anions. The molecular dimensions of the hydrogen bonds are given in Table 4.

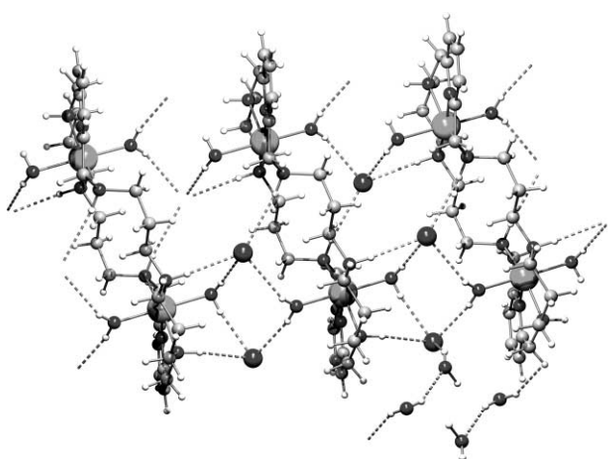

Fig. 5 View of crystal-packing diagram of the complex $[Ni_2([28]py_2N_6)(H_2O)_4]Cl_4\cdot 3H_2O$, **1**, along the *b* crystallographic axis showing the 2-D hydrogen bonding network.

NMR spectroscopic data in solution. Suitable crystals for X-ray diffraction of the Zn^{2+}, Cd^{2+} and Pb^{2+} complexes with $Me_2[28]py_2N_6$ could not be obtained, however the ^{1}H NMR spectra of these complexes were acquired in D_2O (Table 5) and gave some insight into their structures in solution. The spectra of the Ni^{2+} complexes were also studied by ^{1}H NMR spectroscopy. The spectral assignments, made by TOCSY, ROESY and HMQC experiments, correspond to the labelling shown in Scheme 1.

The ^{1}H NMR spectra of all complexes, except the Ni^{2+} and Zn^{2+} complexes in 1 : 1 ratio which will be described later, show seven resonances (Table 5) over the range of temperatures studied (282–298 K): a triplet and a doublet for the H_a and H_b protons of the pyridine ring, one singlet for the H_c protons, two triplets (broad singlets in some complexes) for the H_d and H_f protons, one singlet for the H_g protons and one quintuplet (broad singlet in some cases) corresponding to the H_e protons. The exchange of NH for ND in D_2O is complete and the N–H resonances do not appear. The resonances become only slightly broader with an increase in temperature, and cadmium or lead satellites could not be observed ($^{111/113}$Cd, I = 1/2, 25% natural abundance and ^{207}Pb, I = 1/2, natural abundance 22.6%). All the geminal protons show chemical and magnetic equivalence that

Table 5 ^{1}H NMR data for compound $Me_2[28]py_2N_6$ and its Ni^{2+}, Zn^{2+}, Cd^{2+} and Pb^{2+} complexes in D_2O at 300 K (δ, ppm).[a] For numbering of the atoms see Scheme 1

Compound	pD*	a	b	c	d	e	f	g
$Me_2[28]py_2N_6$	6.19	7.957 (t)	7.488 (d)	4.527 (s)	3.376 (m)	2.362 (q)	3.376 (m)	2.975 (s)
	7.23	7.918 (t)	7.451 (d)	4.468 (s)	3.261 (m)	2.278 (q)	3.261 (m)	2.868 (s)
	7.77	7.882 (t)	7.388 (d)	4.144 (s)	2.952 (m)	1.952 (q)	2.952 (m)	2.570 (s)
	8.82	7.850 (t)	7.346 (d)	3.968 (s)	2.877 (m)	1.849 (q)	2.877 (m)	2.561 (s)
	9.97	7.818 (t)	7.319 (d)	3.838 (s)	2.551 (t)	1.649 (q)	2.461 (t)	2.252 (s)
	10.18	7.811 (t)	7.332 (d)	3.822 (s)	2.519 (t)	1.632 (q)	2.393 (t)	2.202 (s)
	10.53	7.813 (t)	7.316 (d)	3.821 (s)	2.502 (t)	1.606 (q)	2.362 (t)	2.177 (s)
	11.03	7.809 (t)	7.333 (d)	3.812 (s)	2.487 (t)	1.604 (q)	2.328 (t)	2.153 (s)
	11.35	7.809 (t)	7.314 (d)	3.809 (s)	2.470 (t)	1.575 (q)	2.294 (t)	2.125 (s)
	12.06	7.808 (t)	7.312 (d)	3.808 (s)	2.469 (t)	1.574 (q)	2.286 (t)	2.119 (s)
$[Cd(Me_2[28]py_2N_6)]^{2+}$ (1 : 1)	9.01	7.910 (t)	7.396 (d)	4.126 (s)	3.057 (s, br)	2.081 (s, br)	2.958 (s, br)	2.713 (s)
	10.17	7.917 (br)	7.397 (d)	3.963 (s, br)	2.751 (s, br)	1.853 (s, br)	2.751 (s, br)	2.361 (s)
	11.05	7.902 (t)	7.385 (d)	3.908 (s)	2.668 (s, br)	1.762 (s, br)	2.519 (s, br)	2.229 (s)
$[Pb(Me_2[28]py_2N_6)]^{2+}$ (1 : 1)	10.03	7.810(t)	7.328 (d)	3.832 (s)	2.545 (t)	1.654 (q)	2.441(t)	2.239(s)
$[Ni_2(Me_2[28]py_2N_6)]^{4+}$ (2 : 1)	9.30	7.831 (t)	7.316 (d)	3.928 (s)	2.634 (s, br)	1.786 (br)	2.936 (br)	2.546 (s)
	10.50	7.760 (t)	7.244 (d)	3.852 (s)	2.563(s, br)	1.696 (br)	2.856 (br)	2.476 (s)
$[Zn_2(Me_2[28]py_2N_6)]^{4+}$ (2 : 1)	9.71	8.148 (t)	7.561 (d)	4.195 (s)	3.131 (s, br)	2.218 (s, br)	3.050 (s, br)	2.797 (s)
	10.15	7.971 (t)	7.399 (d)	4.076 (s)	2.911 (s, br)	1.885 (s, br)	2.523 (s, br)	2.264 (s)
	11.03	7.971 (t)	7.399(d)	4.073 (s)	2.872 (s, br)	1.870 (s, br)	2.512 (s, br)	2.109 (s)
	11.63	7.998(t)	7.415 (d)	4.083 (s)	2.873 (s, br)	1.875 (s, br)	2.539 (s, br)	2.276 (s)
$[Cd_2(Me_2[28]py_2N_6)]^{4+}$ (2 : 1)	8.73	7.939(t)	7.394(d)	4.060 (s)	2.910 (s, br)	2.152 (s, br)	3.105 (s, br)	2.761 (s)
	10.45	7.942 (t)	7.403 (d)	3.985 (s, br)	2.670 (s, br)	1.889 (s, br)	2.792 (s, br)	2.314 (s)
$[Pb_2(Me_2[28]py_2N_6)]^{4+}$ (2 : 1)	9.65	7.847(t)	7.354 (d)	3.907 (s)	2.692 (m)	1.773 (q)	2.692 (m)	2.468 (s)

[a] Chemical shifts referenced to 3-(trimethylsilyl)-propanoic acid-d_4-sodium salt (0.000 ppm).

can be explained by considering a dynamic process between two energetically favoured conformations.

All the dinuclear complexes show the same sets of resonances as the free ligand and all are shifted to low field (at similar pD values). For protons H_a to H_e there is a general trend when comparing the magnitude of the shifts for the different metal complexes; Zn>Cd>Pb, and more specifically protons H_c to H_g shift more than H_a and H_b for each of the complexes. The larger shifts seen for Zn (H_d–H_f have shifts of *ca.* 0.4–0.5 ppm) are a result of its smaller size which results in shorter M–N bond lengths and greater ligand conformational change on complexation. The resulting complex must be symmetric as only one set of peaks is seen for all protons or there is fast exchange between two asymmetric conformations. Interestingly the resonances for the Cd complex are broadened suggesting that a chemical exchange process is occurring. As the metal size is increased the shifts are markedly reduced due to longer M–N bonds.

The dinuclear Ni complex is particularly interesting as it is diamagnetic. Octahedral or tetrahedral co-ordination in a d^8 complex should result in a paramagnetic $S = 1$ configuration. As this is not observed square planar co-ordination must be occurring in contrast with the X-ray structure of this complex. The larger shifts seen for protons H_f and H_g may result from a greater inductive effect due to square planar co-ordination and/or a conformational change at the ligand backbone. It appears that in solution the two axial water molecules are not present or are far enough apart to produce tetragonal distortion.

In the case of the 1 : 1 solution of Cd^{2+} and $Me_2[28]py_2N_6$ all seven resonances shift downfield when the complex is formed with protons H_d–H_g shifting approximately 0.25–0.46 ppm and the H_a–H_c protons shifting only ≈ 0.2 ppm. This implies that the mononuclear complex involves all the donor atoms of the ligand or most probably involves a dynamic process that occurs between species involving different arrangements of the macrocyclic backbone and different co-ordination spheres but where, on average, all the N-donors are co-ordinated to the metal.

The 1 : 1 solutions of Ni^{2+} and Zn^{2+} complexes with $Me_2[28]py_2N_6$ exhibit more complicated spectra. The nickel complex presents signals from the free ligand and also resonances from a paramagnetic species which can be attributed to the ML complex, as indicated by the distribution diagram (Fig. 2). The paramagnetic species (with a magnetic moment of 3.30 μ_B) exhibits 12 broad contact and pseudo-contact shifted resonances in the 220 to 70 ppm region, a group of 12 sharp resonances between 20 and 60 ppm and approximately 12 in the 0 to 10 ppm region. As the ML complex is paramagnetic it must involve co-ordination that is not square planar. The assignment of these peaks is in progress. The spectrum of the 1 : 1 solution of Zn^{2+} complexes with $Me_2[28]py_2N_6$ is quite complex at a pD of around 9, but as the pD is raised (11.03) the presence of three main species can be detected. This is in agreement with the distribution of species and can be assigned to the free ligand, the $M_2L(OH)_2$ and ML complexes. The superimposition of the spectra of the free ligand and that of the 2 : 1 complex at the same pD allowed the assignment of the resonances corresponding to these species: 1.604 (H_e), 2.153 (H_g), 2.328 (H_f), 2.487 (H_d), 3.812 (H_c), 7.333 (H_b) and 7.809 (H_a) ppm were assigned to the free ligand, and those at 1.870 (H_e), 2.109 (H_g), 2.512 (H_f), 2.872 (H_d), 4.073 (H_c), 7.399 (H_b) and 7.971 (H_a) ppm were assigned to the dinuclear complex. The remaining resonances were assigned to the mononuclear complex: 1.796 (m, H_e), 2.110 (H_g), 2.612 and 2.897 (H_f and H_d), 3.949 (H_c), one pair of doublets at 7.439 and 7.500 ($H_{b,b'}$) and 8.051 (H_a) ppm. The spectrum of the ML species indicates a less labile complex and, as two pairs of doublets are seen for the H_b protons on the pyridine ring, a non-symmetric arrangement can be expected.

UV-vis of the nickel(II) and copper(II) complexes and EPR spectra of the copper(II) complexes. The electronic spectrum of the blue solution of $[Ni(Me_2[28]py_2N_6)]^{2+}$ exhibits three main bands at 960, 610 and 375 nm and several shoulders (*cf.* Table 6). This spectrum and the value of the magnetic

Table 6 Spectroscopic UV-vis-near IR data for $Me_2[28]py_2N_6$ and its Ni^{2+} and Cu^{2+} complexes (T = 25.0 °C)

Complex (M : L ratio) (colour)	pH	UV-vis-near IR Absortion max/nm (ε_{molar}/dm^3 mol^{-1} cm^{-1})
$[Ni(Me_2[28]py_2N_6)]^{2+}$ (1 : 1) (light blue)	10.70	1144 (sh., 2.2); 960 (5.0); 768 (sh., 1.2); 610 (1.3); 375 (sh., 232.2); 270 (sh., 732.7); 264 (883.1)
$[Ni_2(Me_2[28]py_2N_6)]^{4+}$ (2 : 1) (light green)	8.50	1137 (sh., 0.9); 959 (2.2); 756 (sh., 0.6); 612 (0.7); 270 (sh., 259.2); 264 (326.4)
$[Cu(Me_2[28]py_2N_6)]^{2+}$ (1 : 1) (light blue)	10.06	622 (255.4); 580 (sh., 218.5); 300 (sh., 4523.6); 262 (16709.8)
$[Cu_2(Me_2[28]py_2N_6)]^{4+}$ (2 : 1) (blue)	7.70	650 (145.8); 580 (sh., 106.4); 288 (sh., 3339.2); 262 (7565.0)
$(Me_2[28]py_2N_6)$	5.00	262 (5247.4)
	11.50	266 (8983.7)

Table 7 Spectroscopic X-band EPR data for the Cu^{2+} complexes of $Me_2[28]py_2N_6$ 1 : 1 ratio, and other complexes with similar structure

Complex	Visible band λ_{max}/nm	EPR parameters						Ref.
		g_x	g_y	g_z	A_x^*	A_y^*	A_z^*	
$[Cu(Me_2[28]py_2N_6)]^{2+}$	622	2.029	2.072	2.222	11.6	21.0	170.3	[a]
$[Cu([18]py_2N_4)]^{2+}$	667	2.051	2.083	2.244	33.0	17.4	160.0	[a]
$[Cu(Me[14]pyN_3)]^{2+}$	560	2.034	2.060	2.188	0.5	3.4	192.9	[b]
$[Cu(py_2[14]pyN_3)]$	661	2.036	2.086	2.220	5.7	19.7	172.6	[a]

$A_i \times 10^4$ cm^{-1}. [a] Present work. [b] Ref. 23.

moment (3.30 μ_B) are consistent with tetragonally distorted octahedral symmetry.[18] Indeed, the three bands of low intensity correspond to the three spin allowed transitions of a d^8 metal centre complex with octahedral symmetry and the reduction of symmetry to tetragonal leads to additional d-orbital splittings or band broadening.[18,19] An increase in the amount of nickel to form the dinuclear complex does not lead to significant changes in the electronic spectrum, and in fact the X-ray structure confirms the octahedral arrangement around each nickel center.

The copper(II) complex of $Me_2[28]py_2N_6$ at the 1 : 1 ratio exhibits a broad band in the visible region with the maximum centred at 622 nm, see Table 6. The X-band EPR spectrum of this complex at low concentrations (≈ 1×10^{-3} mol dm^{-3}) was obtained in a mixture of H_2O–DMSO (1 : 1) at 100 K. The spectrum exhibits three well-resolved lines at low field without superhyperfine splitting. A strong and not resolved band in the high field region of the spectrum overlaps the fourth line. The hyperfine coupling constants (A) and g values of glassy solutions of this complex, obtained by simulation of the spectra[20] are presented in Table 7. These values are typical of copper(II) complexes in rhombic symmetry axially elongated and a $d_{x^2-y^2}$ ground state, consistent with elongated rhombic-octahedral or distorted square-based pyramidal geometries.[21,22] The EPR parameters, together with the maximum of the d–d absorption band, of $[Cu(Me_2[28]py_2N_6)]^{2+}$ indicate a hexa-co-ordinate environment for the copper. Indeed, this complex presents higher g_z, lower A_z parameters and a red shift of the visible band when compared with the corresponding values of $[Cu(Me[14]pyN_3)]^{2+}$,[23] see Table 7, which exhibits a square-planar structure as shown by X-ray diffraction analysis.[24] Additionally, the $[Cu(Me_2[28]py_2N_6)]^{2+}$ complex exhibits electronic parameters similar to those of $[Cu(py_2[14]pyN_3)]^{2+}$ and $[Cu([18]py_2N_4)]^{2+}$. In the latter complex the copper adopts an octahedral geometry.[3] The crystal structure of the copper(II) complex with $py_2[14]pyN_3$ is not available, but that of nickel exhibits an elongated *cis*-octahedral geometry.[25,26] The electronic parameters also reveal that $[Cu([18]py_2N_4)]^{2+}$ has a stronger ligand field than that of $[Cu(Me_2[28]py_2N_6)]^{2+}$, which is much closer to that of $[Cu(py_2[14]pyN_3)]^{2+}$.

Molecular modelling. The solution studies of the co-ordination behaviour of $Me_2[28]py_2N_6$ showed that it is capable of binding to one or two metal centres. As mentioned above it was impossible to obtain suitable crystals of the mononuclear complexes for X-ray diffraction studies. So, in order to understand the structural preferences of $[28]py_2N_6$ (or $Me_2[28]py_2N_6$) in mononuclear complexes, theoretical calculations were carried out by MM and MD using the universal force field.[27] It was assumed that the influence of the *N*-methyl groups is marginal and so all calculations were carried out on $[28]py_2N_6$. The evaluation of the co-ordination behaviour of this type of macrocycle is not a trivial task due to the large dimensions and the number of donor atoms involved. Indeed the macrocycle is sterically flexible and can adopt several different co-ordination modes. The influence of the metal ion size on the structural preferences of the ligand was also investigated.

The modelling studies started with a conformational search of the metal complexes $[M([28]py_2N_6)]^{2+}$, using quenched dynamics techniques. In agreement with the solution studies, two starting model complexes, $[M([28]py_2N_6)]^{2+}$ (M = Ni^{2+} and Cd^{2+}), having metals with different stereoelectronic properties were constructed from the crystal structure of **1**. The metal was positioned at the centre of the macrocyle and no bonds between the metal and nitrogen donor atoms were included. In this way, the macrocycle should adjust freely to the steric–electronic demands of the metal centre, without any bond distance and angle constraints. Each model was minimised by MM and subsequently subjected to MD simulation (see Experimental section). 1000 conformations were saved in each trajectory file and were used to investigate the co-ordination modes of $[28]py_2N_6$ in hexa- and octa-co-ordinated environments.

Taking into account the symmetry of the macrocycle, 10 different co-ordination modes were obtained for the hexa-co-ordinated complexes (**a–j**, see Scheme 2). By contrast, only one configuration (isomer **k**) was obtained with a co-ordination number 8, which involved the binding of all nitrogen donors. Upon co-ordination the *N*-aliphatic nitrogen atoms of the macrocycle become chiral centres and the conformations can therefore be described using the *RS* nomenclature.

For hexa-co-ordination, the M–N bonds of the frames saved in the trajectory files were rebuilt taking into account each arrangement presented in Scheme 2 and all structures were minimised by MM but with an octahedral co-ordination environment imposed upon the metal atom. The lowest energy conformations found for each geometric isomer are listed in Table 8, and the structures for the cadmium isomers are shown in Fig. 6. It was found that all co-ordination modes lead to an identical disposition of nitrogen atoms around the metal centre in the lowest energy forms for both metals (Ni and Cd), except in **d** where the cadmium isomer has the nitrogen atoms of the pyridine rings adopting a *cis* disposition subtending an angle of 104.5° (isomer **d1**) at the metal center. In the nickel isomer they are *trans* with an angle N(sp^2)–Ni–N(sp^2) of 173.9° (isomer **d2**). However, in the next lowest energy conformation for the nickel

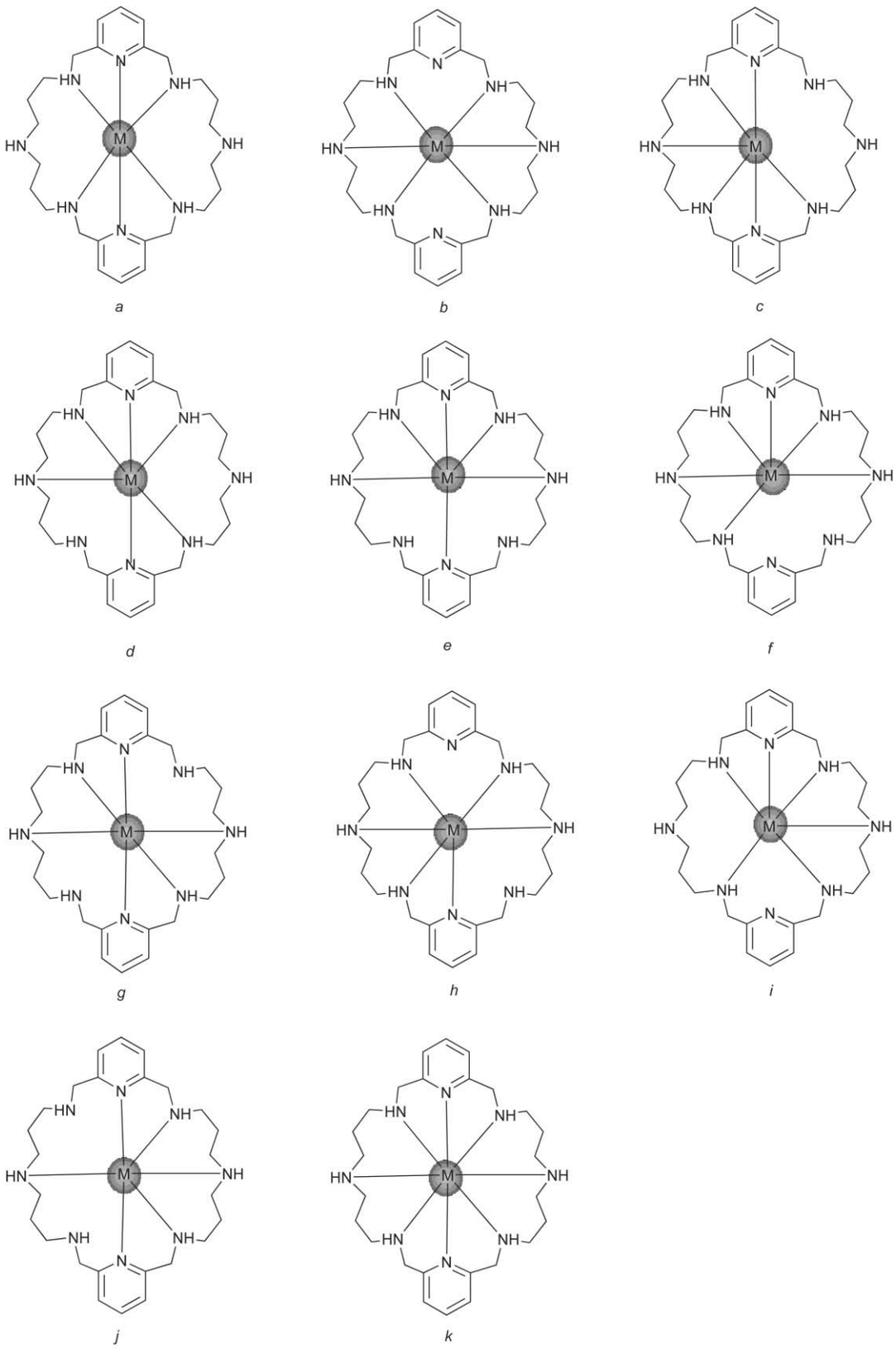

Scheme 2

complex, the co-ordinated nitrogen donors adopt an arrangement of the type **d1** while for the cadmium the arrangement is of type **d2** and for both metals the energy difference between the **d1** and **d2** arrangements is small (see Table 8). The bending terms of the angles subtended at the metal centre were described using a cosine periodic function, which incorporates the possibility that the angles subtended to the metal centre take more than one ideal value, *e.g.* 90° or 180°, see Experimental section. Therefore, the spatial disposition of the nitrogen donors around the metal centre is not pre-defined and either *cis* or *trans* arrangements can be adopted. Two conformational isomers with a co-ordination mode of type **d** are possible suggesting that, in this particular case, the size of the metal ion determines the spatial arrangement of the donor atoms in the metal co-ordination sphere.

Table 8 Lowest energy conformations found for hexa-co-ordinated $[M([28]py_2N_6)]^{2+}$ (M = Ni^{2+} or Cd^{2+})

Geometric isomer	Energy/kcal mol^{-1}		λ/°		N(sp^2)–M–N(sp^2)/°	
a	163.41	*144.86*	75.5	*59.4*	178.8	*177.4*
b	308.93	*138.04*				
c	128.50	*115.90*			96.9	*100.1*
d1	181.91	*138.40*			96.3	*104.5*
d2	177.89	*140.90*	53.8	*51.4*	173.9	*164.5*
e	208.50	*136.46*	18.2	*40.9*	178.1	*176.8*
f	143.40	*109.97*				
g	186.82	*132.90*			97.8	*102.8*
h	247.38	*132.96*				
i	207.05	*132.78*				
j	179.30	*122.00*			94.6	*98.5*

λ is the dihedral angle between the pyridine rings and was measured when the macrocycle adopts a helical topology. In italic are the values for the Cd^{2+} isomers.

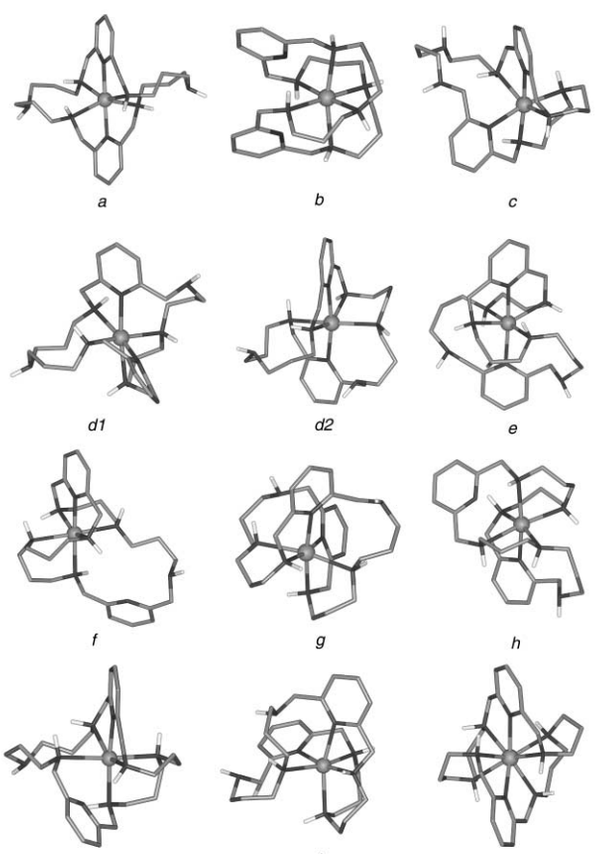

Fig. 6 Lowest energy conformations found for $[Cd([28]py_2N_6)]^{2+}$. Hydrogen atoms bonded to carbon atoms are removed for clarity.

The **a**, **d1** and **e** conformations involve the binding of both pyridine rings in axial positions leading to helical topologies with angles between the two pyridine rings of 75.5, 53.8 and 18.2°, respectively, for nickel (for cadmium the values are 59.4° for **a** and 40.9° for **e**, the **d2** conformation for this metal is not a helical form, see above). However, rather unexpectedly these conformers are not the most stable, see Table 8. Indeed, X-ray structures of metal complexes involving large tetraimine macrocycles (30- and 40-membered rings and containing 6 or more donor atoms) and small metal ions such as Fe^{2+} (refcode PYRFEA), Co^{2+} (refcodes LETZAL and PYRFEB), Ni^{2+} (refcodes LETZEP and NORDED) and Zn^{2+} (refcode LETZIT) have been determined and all show a co-ordination mode of type **a**.

The lowest energy conformation for nickel is **c** followed by **f**. The remaining conformations exhibit higher energies and the energy differences indicate that they are unlikely to be observed. For cadmium conformations **c** and **f** are reversed in the energy ranking, followed by **j**. Furthermore, the remaining conformations have similar energies around 20 kcal mol^{-1} higher, apart from **a** and **b** which are *ca*. 30 kcal mol^{-1} above the lowest energy forms, see Table 8.

It is interesting to note that the lowest energy conformations **c** and **f**, for both metals have the six donor atoms in consecutive positions in the macrocyclic backbone. This ensures that the metal is accommodated to one side of the macrocycle, suggesting that the cavity provided by the whole macrocycle is too large to encapsulate the metal centre, even a metal with a large ionic size, such as cadmium. Therefore these conformations correspond to asymmetrical co-ordination modes, see Scheme 2. By contrast, conformation **j** for cadmium also corresponds to an asymmetric co-ordination mode but here the two non-co-ordinated nitrogen atoms are not adjacent but separated by one donor nitrogen atom.

The highest co-ordination number involves the binding of all eight nitrogen donors and obviously only one possible M–N bond pattern is possible. The most common geometric arrangements for eight-co-ordinated structures are the square antiprism and dodecahedron.[4] However it is difficult to find the correct analytical form for the functions to use to describe the bending angle terms centred at the metal for these two geometries in $[M([28]py_2N_6)]^{2+}$ using only two atom types for nitrogen donors: N_R and N_3 for sp^2 and sp^3 nitrogen donors, respectively.

An approximate way to model the eight-co-ordinated polyhedron, it is to minimise the structures with M–N distances constrained and excluding the bond angle terms involving the metal atom from the force field. This procedure was adopted leading to energies for the lowest energy conformations of 286.97 kcal mol^{-1} for nickel and of 112.77 kcal mol^{-1} for cadmium. Of course these energies cannot be directly compared with those for co-ordination number six quoted in Table 8, which have a large contribution to the bending angle terms subtended at the metal centre. In fact, when these conformations are optimized with a N–M–N force constant of 0 kcal mol^{-1} rad^{-2} their energies decrease considerably and are much lower than those found for eight-co-ordination, except in the case of **b** which takes the values of 281.26 kcal mol^{-1} for nickel and 120.96 kcal mol^{-1} for cadmium.

The last type of calculation involved the evaluation of the hole-size cavity provided by each of the 11 hexa-co-ordinate conformations described above. The steric energy profiles were calculated by our published method.[3,17,24,28] The M–N distances were fixed at specific values using a large force constant and the remainder of the structure is allowed to converge to the lowest possible energy, thus giving a plot of the energy *versus* M–N distance, which is independent of the metal ion considered. Charges were not included since they only have a marginal impact in this type of calculation. This methodology has been extensively applied to the calculation of macrocyclic cavities and for the prediction of structures of macrocyclic systems.[29] In addition, the M–N(sp^3) and M–N(sp^2) distances were changed

concomitantly by 0.05 Å between the limits of 1.8 and 2.8 Å and a difference of 0.1 Å was kept between them. This is consistent with the X-ray data available for metal complexes containing azamacrocycles incorporating pyridine moieties.[4] The results are shown in Fig. 7 for all conformations.

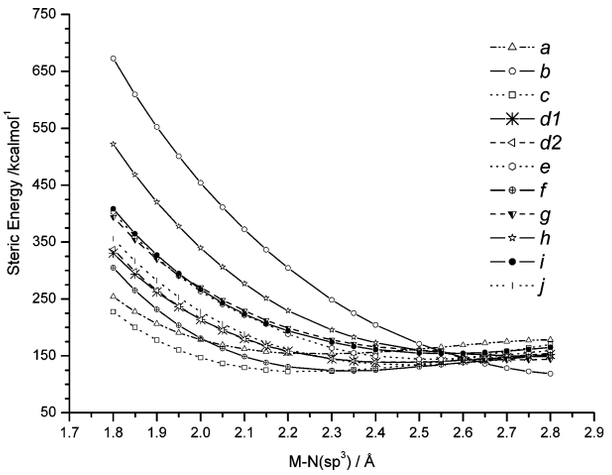

Fig. 7 Plot of the steric energy *versus* M–N(sp^3) for hexa-co-ordinated $[M([28]py_2N_6)]^{n+}$ isomers.

All geometric isomers present broad energy profiles with a sharp energy increase for shorter M–N distances. By contrast, for larger distances, all isomers except **b**, exhibit smooth energy variations suggesting that this ligand is particularly suitable for the formation of mononuclear species with larger metal ions. **c** is the most stable conformer at distances less then 2.35 Å, at which distance the **f** conformer becomes slightly more stable. The **a** isomer curve is intermediate in energy between those for **f** and **c** isomers up to 2.05 Å. For distances up to 2.25 Å, the remaining isomers are barely distinguishable, suggesting that any of these bonding patterns could be adopted.

For the eight-co-ordinate structure (isomer **k**, see Scheme 2), as mentioned above, it is quite difficult to constrain the geometry in terms of angle bending terms, so for comparison purposes the curves for co-ordination number six are also calculated using a force constant of 0 kcal mol^{-1} rad^{-2}. For distances up to 2.5 Å, the eight-co-ordinated isomer presents a high steric strain, considerably higher than for the hexa-co-ordinated structures, but for higher distances this form has only slightly higher energy than the hexa-co-ordinated conformations.

Conclusions

This work has shown that the 28-membered macrocycle, $[28]py_2N_6$ and its *N*-methyl derivative, due to their large cavity size and the high number of nitrogen donors, are particularly suitable for the co-ordination of two metal centres in dinuclear complexes. Our potentiometric and NMR results revealed that in solution mononuclear species are predominant for Ni^{2+}, Zn^{2+} and Cd^{2+} in a 1 : 1 ratio, while for Pb^{2+} the dinuclear species predominates even for the 1 : 1 ratio. The EPR of the mononuclear species, $Cu(Me_2[28]py_2N_6)$, suggested that an octahedral complex is formed involving the binding of six nitrogen donors. In this context, the capability and selectivity of $[28]py_2N_6$ to encapsulate metal ions with different stereoelectronic requirements in mononuclear species with six- (octahedral geometric arrangement) and eight-co-ordination environment were evaluated theoretically. As expected, the results indicated that this type of macrocycle is particularly adequate for the accommodation of large metal ions. Additionally, for a hexa-co-ordinate environment two geometric arrangements were favoured sterically, **c** and **f**. In the latter case the steric strain is alleviated by leaving a pyridine ring and the contiguous nitrogen free, while in the former, both pyridine rings are co-ordinated adopting a *cis* disposition.

In the present work, the formation of mononuclear species has been mainly investigated. However, dinuclear species become important as the metal ion concentration increases, in agreement with the crystal structure of $[Ni_2([28]py_2N_6)(H_2O)_4]^{4+}$. Additionally, our potentiometric studies reveal that the dinuclear species predominance depends on the metal ion size. These conclusions are not necessarily inconsistent with our theoretical studies which suggest that this macrocycle is able to encapsulate large metal ions in mononuclear complexes. In this context the theoretical study of the co-ordination of two metal centres into large macrocyclic cavities is in progress in our laboratory.

Experimental

Microanalyses were carried out by the ITQB Microanalytical Service. IR spectra were recorded from KBr pellets on a UNICAM Mattson 7000 spectrometer.

Reagents

2,6-Pyridinedimethanol was obtained from Aldrich, 2,6-pyridinedicarbaldehyde was prepared by a published method,[30] 3,3-diamine-*N*-methyldipropylamine and bis(3-aminopropyl)amine were obtained from Aldrich. All the chemicals were of reagent grade and used as supplied without further purification. The reference used for the ^{1}H NMR measurements in D_2O was 3-(trimethylsilyl)-propanoic acid-d_4-sodium salt and in $CDCl_3$ the solvent itself. For ^{13}C NMR spectra 1,4-dioxane was used as internal reference.

Syntheses

3,7,11,19,23,27,33,34-Octaazatricyclo-[27.3.1.1.^{13,17}]-tetratriacontane-1(32),13(14),15,17,29,31-hexaene, [28]py$_2$N$_6$, or of its 7,23-dimethyl derivative (Me$_2$[28]py$_2$N$_6$). Bis(3-aminopropyl)-amine (0.528 g, 4.0 mmol) [or 3,3-diamine-*N*-methyldipropylamine (0.532 g, 4.0 mmol)] was dissolved in acetonitrile (100 cm^3) and 2,6-pyridinedicarbaldehyde (0.55 g, 4.0 mmol) in acetonitrile (60 cm^3) was added in small portions during 4 h. The resulting mixture was concentrated to 40 cm^3 under vacuum. The yellow precipitate of the macrocyclic Schiff base was filtered off and dissolved in ethanol (25 cm^3). $NaBH_4$ (1.1 g, 29 mmol) was then added in small portions at room temperature. At the end of the reaction (when the effervescence stopped), the ethanol was removed and the remaining yellow product was dissolved in water (40 cm^3). The pH of the aqueous solution was increased to 12 with NaOH and several extractions with chloroform (6 × 50 cm^3) were carried out. The organic phases were combined and completely evaporated under vacuum. The oil corresponding to the desired product was precipitated in the form of a white HCl-salt easily filtered off after 12 h at low temperature. Yield: 69.5% ([28]py$_2$N$_6$) and 80.3% (Me$_2$[28]py$_2$N$_6$). [28]py$_2$N$_6$: mp 205–7 °C (decomp.). ^{1}H NMR (D_2O): δ 2.32 (8 H, q, $NCH_2CH_2CH_2N$), 3.34 (16 H, m, $NCH_2CH_2CH_2N$), 4.52 (8 H, s, $pyCH_2N$), 7.50 (4 H, d, py) and 7.96 (2 H, t, py). ^{13}C NMR (D_2O): δ 23.3 ($NCH_2CH_2CH_2N$), 44.8 ($NCH_2CH_2CH_2N$), 45.1 ($NCH_2CH_2CH_2N$), 51.4 ($pyCH_2N$), 123.7 (py), 139.9 (py) and 151.1 (py). Found: C, 40.04; H, 7.92; N, 14.65%. Calc. for $C_{26}H_{44}Cl_6N_8\cdot H_2O$: C, 40.12; H, 7.76; N, 14.53%. IR (KBr pellets, cm^{-1}): 3410, 3074, 2720, 1629, 1578, 1552, 1446, 998, 791. Me$_2$[28]py$_2$N$_6$: mp 197–8 °C (decomp.). ^{1}H NMR (D_2O): δ 2.05 (8 H, q, $NCH_2CH_2CH_2N$), 2.6 (6 H, s, NCH_3), 3.1 (16 H, m, $NCH_2CH_2CH_2N$), 4.3 (8 H, s, $pyCH_2N$), 7.5 (4 H, d, py) and 7.95 (2 H, t, py). ^{13} C NMR (D_2O): δ 21.7 ($NCH_2CH_2CH_2N$), 41.5 ($NCH_2CH_2CH_2N$), 45.1 (NCH_3), 51.5 ($NCH_2CH_2CH_2N$), 53.1 ($pyCH_2N$), 123.6 (py), 139.9 (py) and 151.1 (py). Found: C, 43.99; H, 8.05; N, 14.59%. Calc. for $C_{28}H_{48}Cl_6N_8\cdot 3H_2O$: C, 43.79; H, 7.85; N, 14.59%. IR

(KBr pellets, cm^{-1}): 3430, 2974, 2810, 1598, 1579, 1556, 1437, 1020, 792.

$[Ni_2([28]py_2N_6)(H_2O)_4]Cl_4 \cdot 3H_2O$ 1. An aqueous solution of $NiCl_2 \cdot 6H_2O$ (0.12 mmol, 0.0285 g) was added to a stirred solution of $[28]py_2N_6$ (0.06 mmol, 0.050 g) dissolved in a minimum volume of water (≈ 2 cm^3). The mixture was stirred for 2 h, the solvent was removed under vacuum and the mixture taken up in methanol. The precipitate formed was filtered off and the solvent removed. The pure complex was dissolved in deuterium oxide. Dark blue crystals were formed in five days by slow evaporation of the solvent at room temperature. Yield: ≈ 85%: C, 36.7; H, 6.8; N, 13.3%. Calc. for $C_{26}H_{58}Cl_4N_8Ni_2O_7$: C, 36.57; H, 6.85 N, 13.12%.

Potentiometric measurements

Reagents and solutions. Metal ion solutions were prepared at about 0.025 mol dm^{-3} from nitrate salts, of analytical grade with demineralized water (obtained by a Millipore/Milli-Q system) and were standardised as described.[3,28] Carbonate-free solutions of the titrant, KOH, were obtained, maintained and discarded as described.[3,28]

Equipment and work conditions. The equipment used has been described previously.[3,28] The temperature was kept at 25.0 ± 0.1 °C; atmospheric CO_2 was excluded from the cell during the titration by passing purified nitrogen across the top of the solution in the reaction cell. The ionic strength was kept at 0.10 mol dm^{-3} with KNO_3.

Measurements. The $[H^+]$ of the solutions was determined by the measurement of the electromotive force of the cell, $E = E'^{o} + Q\lg[H^+] + E_j$. E'^{o}, Q, E_j and $K_w = ([H^+][OH])$ were obtained as described previously.[3,28] The term pH is defined as $-\log [H^+]$. The value of K_w was found to be equal to $10^{-13.80}$ $mol^2\ dm^{-6}$.

The potentiometric equilibrium measurements were carried out using 20.00 cm^3 of ≅ 2.50×10^{-3} mol dm^{-3} ligand solutions diluted to a final volume of 30.00 cm^3, in the absence of metal ions and in the presence of each metal ion for which the $c_M : c_L$ ratios were 1 : 1 and 2 : 1. A minimum of four replicate measurements was taken.

Calculation of equilibrium constants. Protonation constants

$$K_i^{H} = \frac{[H_iL]}{[H_{i-1}L][H]}$$

were calculated by fitting the potentiometric data obtained for the free ligand to the HYPERQUAD program.[31] Stability constants of the various species formed in solution were obtained from the experimental data (potentiometric titrations) corresponding to the titration of solutions of different metal ions to ligand ratios, also using the HYPERQUAD program. The initial computations were obtained in the form of overall stability constants, $\beta_{M_mH_hL_l}$ values,

$$\beta_{M_mH_hL_l} = \frac{[M_mH_hL_l]}{[M]^m[L]^l[H]^h}$$

Mononuclear species, ML, MH_iL (i = 1–4), $MH_{-1}L$, and also dinuclear species, M_2L, M_2H_jL (j = 1, 2), $M_2H_{-1}L$ and $M_2(H_{-1})_2L$, were found for most of the metal ions studied with $Me_2[28]py2N_6$ (being $\beta_{MH_{-1}L} = \beta_{ML(OH)} \times K_w$, $\beta_{M_2H_{-1}L} = \beta_{M_2L(OH)} \times K_w$, and $\beta_{M_2(H_{-1})_2L} = \beta_{M_2L(OH)_2} \times (K_w)^2$). Differences, in log units, between the values of protonated or hydrolysed and non-protonated constants, for the monomer and dimer reactions respectively, provide the stepwise reaction constants. The species considered in a particular model were those that could be justified by the principles of co-ordination chemistry. The errors quoted are the standard deviations of the overall stability constants given directly by the program for the input data, which include all the experimental points of all titration curves. The standard deviations of the stepwise constants, shown in Table 2, were determined by normal propagation rules.

The stability constants for each metal ion were determined from a minimum of 120 (for the Ni^{2+} complex) to 210 (for the Cu^{2+} complex) experimental points (2 to 4 titration curves).

Spectroscopic studies

^1H and ^{13}C NMR spectra were recorded on a Bruker CXP-300 or a Bruker DRX-500 spectrometer. Solutions of the ligands and respective complexes for the measurements (≈ 0.01 mol dm^{-3}) in D_2O were made up and the pD was adjusted by addition of DCl or CO_2-free KOD with a Orion 420A instrument fitted with a combined Ingold 405M3 microelectrode. The $-\log [D^+]$ was measured directly in the NMR tube, after the calibration of the microelectrode with buffered aqueous solutions. The final pD was calculated from pD = pH* + 0.40.[32] The value of pH* corresponds to the reading of the pH meter previously calibrated with two standard aqueous buffers at pH 4 and 7. Electronic spectra of the complexes in water were recorded with a UNICAM model UV-4 (in the UV-vis range) or a Shimadzu model UV-3100 spectrophotometers (in the near IR range). EPR spectroscopy measurements of the Cu^{2+} complexes were recorded with a Bruker ESP 380 spectrometer equipped with continuous-flow cryostats for liquid nitrogen, operating at X-band. The complexes were prepared at 0.001 mol dm^{-3} in water–DMSO (1 : 1) and the spectra were recorded at pH 7.0 and 10.0 for the 1 : 1 ratio M : L solutions at 100 K.

Crystallography

Crystal data for **1**: $C_{26}H_{58}Cl_4N_8Ni_2O_7$, M_r = 854.02. Monoclinic, space group $C2/c$, a = 32.098 (34) b = 16.040 (17), c = 7.471 (8) Å, β = 100.88 (1)°, U = 3777 (7) Å^3, Z = 4, ρ(calc) = 1.502 Mg m^{-3}, μ(Mo-Kα) = 1.331 mm^{-1}. X-Ray data were collected at room temperature on a MAR research plate system using graphite monocromatised Mo-Kα radiation (λ = 0.71073 Å) at Reading University. The crystals were positioned at 70 mm from the image plate. 95 frames were taken at 2° intervals using an appropriate counting time of 10 min. Data analysis was performed with XDS program.[33] Intensities were not corrected for absorption effects.

Intensities of 3563 observations collected were merged in the Laue symmetry 2/m to 2315 independent reflections with a R_{int} of 0.0981.

The structure was solved by direct methods and by subsequent difference Fourier syntheses and refined by full matrix least squares on F^2 using the SHELX-97 system programs.[34] The hydrogen atoms on the parent carbon and nitrogen atoms were included in calculated positions while hydrogen atoms of the water molecules were located from difference Fourier maps and refined with O–H distances and H–O–H angles constrained to 0.82 Å and 104.5°, respectively. Anisotropic thermal parameters were used for all non-hydrogen atoms while the thermal movement of hydrogen atoms was described using isotropic parameters equivalent to 1.2 times those of the atom to which they were attached. The last difference Fourier map calculated the residual electronic density as ranging from 0.742 to −0.517 e Å^{-3} was within expected values. The final refinement of 234 parameters converged to final R and R_w indices R_1 = 0.1043 and wR_2 = 0.2775 for $I > 2\sigma(I)$ and R_1 = 0.1973 and wR_2 = 0.3160 for all data. The ORTEP diagram was drawn with graphical package software PLATON.[35]

CCDC reference number 208896.

See http://www.rsc.org/suppdata/dt/b3/b304381a/ for crystallographic data in CIF or other electronic format.

Molecular modelling

Conformational analyses were undertaken *via* molecular dynamics techniques using the universal force field[27] within the CERIUS2 software.[36] For each metal a molecular dynamics simulation was carried out at 1500 K using a step size of 1 fs and 1000 conformations were collected at 0.25 ps intervals over 250 ps. A constant NVT thermostat with default parameters was used and the equilibration period was 3 ps. The conformations saved in a trajectory file were further minimised by molecular mechanics calculations.

The starting models used in dynamics simulations were built from the X-ray structure of **1** as described above and subsequently minimised by molecular mechanics calculations. The universal force field was slightly modified on the parameters subtended at Cd^{2+} and Ni^{2+} centres, taking into account the single crystal X-ray data available for related macrocycle complexes containing pyridine moieties; thus, ideal distances Ni–N(sp^2) (2.00 Å) and Ni–N(sp^3) (2.10 Å) and Cd–N(sp^2) (2.36 Å) and Cd–N(sp^3) (2.46 Å). The corresponding force constants for M–N stretching and N–M–N bending angle terms were calculated using the appropriated equations given in ref. 27.

Acknowledgements

The authors acknowledge financial support from Fundação para a Ciência e Tecnologia (FCT) and POCTI, with co-participation of the European Community fund FEDER (Project n. POCTI/1999/QUIM/35396).

References

1 M. Mitewa and P. R. Bontchev, *Coord. Chem. Rev.*, 1994, **135/136**, 129.
2 A. Bianchi, M. Micheloni and P. Paoletti, *Coord. Chem. Rev.*, 1991, **130**, 17.
3 L. Branco, J. Costa, R. Delgado, M. G. B. Drew, V. Félix and B. J. Goodfellow, *J. Chem. Soc., Dalton Trans.*, 2002, 3539.
4 (*a*) F. H. Allen, *Acta Crystallogr., Sect. B*, 2002, **58**, 380; (*b*) I. J. Bruno, J. C. Cole, P. R. Edginton, M. Kessler, C. F. Macrae, P. McCabe, J. Pearson and R. Taylor, *Acta Crystallogr., Sect. B*, 2002, **58**, 389.
5 J. Costa, R. Delgado, M. G. B. Drew and V. Félix, to be published.
6 K. I. Dhont, W. Lippens, G. Herman and A. M. Goeminne, *Bull. Chim. Belg.*, 1992, **101**, 1061.
7 D. A. Rockcliffe, A. E. Martell and J. H. Reibenspies, *J. Chem. Soc., Dalton Trans.*, 1996, 167.
8 K. E. Krakowiak, J. S. Bradshaw, W. Jiang, N. K. Dalley, G. Wu and R. M. Izatt, *J. Org. Chem.*, 1991, **56**, 2675.
9 M. G. B. Drew, V. McKee and S. M. Nelson, *J. Chem. Soc., Dalton Trans.*, 1980, 942.
10 M. F. Cabral, B. Murphy and J. Nelson, *Inorg. Chim. Acta*, 1984, **90**, 169.
11 M. G. B. Drew, M. McCann and S. M. Nelson, *J. Chem. Soc., Dalton Trans.*, 1981, 1868.
12 M. G. B. Drew, J. Nelson and S. M. Nelson, *J. Chem. Soc., Dalton Trans.*, 1981, 1678.
13 G. Shangguan, A. E. Martell, Z. Zhang and J. H. Reibenspies, *Inorg. Chim. Acta*, 2000, **299**, 47.
14 A. Bianchi, S. Mangani, M. Micheloni, V. Nanini, P. Orioli, P. Paoletti and B. Seghi, *Inorg. Chem.*, 1985, **24**, 1182.
15 L. D. Pettit and H. K. J. Powell, *IUPAC Stability Constants Database*, Academic Software, Timble, 1993.
16 L. Alderighi, P. Gans, A. Ienco, D. Peters, A. Sabatini and A. Vacca, *Coord. Chem. Rev.*, 1999, **184**, 311.
17 V. Félix, J. Costa, R. Delgado, M. G. B. Drew, M. T. Duarte and C. Resende, *J. Chem. Soc., Dalton Trans.*, 2001, 1462.
18 A. B. P. Lever, *Inorganic Electronic Spectroscopy*, Elsevier, Amsterdam, 2nd edn., 1984.
19 L. Y. Martin, C. R. Sperati and D. H. Busch, *J. Am. Chem. Soc.*, 1977, **99**, 2968.
20 F. Neese, Diploma Thesis, University of Konstanz, June 1993.
21 B. J. Hathaway, *Coord. Chem. Rev.*, 1983, **52**, 87.
22 H. Yokoi, M. Sai, T. Isobe and S. Ohsawa, *Bull. Chem. Soc. Jpn.*, 1972, **45**, 2189.
23 J. Costa, R. Delgado, M. C. Figueira, R. T. Henriques and M. Teixeira, *J. Chem. Soc., Dalton Trans.*, 1997, 65.
24 V. Félix, M. J. Calhorda, J. Costa, R. Delgado, C. Brito, M. T. Duarte, T. Arcos and M. G. B. Drew, *J. Chem. Soc., Dalton Trans.*, 1996, 4543.
25 K. P. Balakrishnan, H. A. A. Omar, P. Moore, N. W. Alcock and G. A. Pike, *J. Chem. Soc., Dalton Trans.*, 1990, 2965.
26 J. Costa, R. Delgado, M. G. B. Drew and V. Félix, *J. Chem. Soc., Dalton Trans.*, 1999, 4331.
27 A. K. Rappe, C. J. Casewit, K. S. Colwell, W. A. Goddard III and W. M. Skiff, *J. Am. Chem. Soc.*, 1992, **114**, 10024.
28 P. Antunes, P. M. Campello, R. Delgado, M. G. B. Drew, V. Félix and I. Santos, *Dalton Trans.*, 2003, 1852.
29 P. Comba and T. W. Hambley, *Molecular Modeling of Inorganic Compounds*, VCH, Weinheim, 1995, pp. 85—88 and references therein.
30 J. Costa and R. Delgado, *Inorg. Chem.*, 1993, **32**, 5257 and cited references.
31 P. Gans, A. Sabatini and A. Vacca, *Talanta*, 1996, **43**, 1739.
32 R. Delgado, J. J. R. Fraústo da Silva, M. T. S. Amorim, M. F. Cabral, S. Chaves and J. Costa, *Anal. Chim. Acta*, 1991, **245**, 271.
33 W. Kabsch, *J. Appl. Crystallogr.*, 1988, **21**, 916.
34 G. M. Sheldrick, SHELX-97, University of Göttingen, Germany, 1997.
35 A. L. Spek, PLATON, A Multipurpose Crystallographic Tool, Utrecht University, The Netherlands, 1999.
36 CERIUS2, version 4.2, Molecular Simulations Inc, San Diego, 2000.